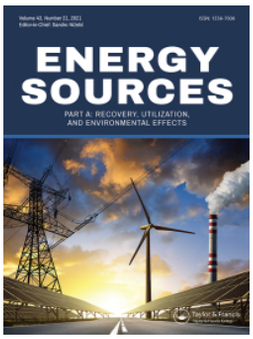

Energy Sources, Part A: Recovery, Utilization, and Environmental Effects

ISSN: 1556-7036 (Print) 1556-7230 (Online) Journal homepage: www.tandfonline.com/journals/ueso20

Investigation effects of different calorific values and operating conditions on biogas flame: a CFD study

Mehmet Salih Cellek, Usame Demir & Gokhan Coskun

To cite this article: Mehmet Salih Cellek, Usame Demir & Gokhan Coskun (2024) Investigation effects of different calorific values and operating conditions on biogas flame: a CFD study, Energy Sources, Part A: Recovery, Utilization, and Environmental Effects, 46:1, 8171-8189, DOI: 10.1080/15567036.2024.2368489

To link to this article: https://doi.org/10.1080/15567036.2024.2368489

ENERGY SOURCES, PART A: RECOVERY, UTILIZATION, AND ENVIRONMENTAL EFFECTS
2024, VOL. 46, NO. 1, 8171–8189
https://doi.org/10.1080/15567036.2024.2368489

Investigation effects of different calorific values and operating conditions on biogas flame: a CFD study

Mehmet Salih Cellek [a], Usame Demir [b], and Gokhan Coskun [c]

[a]Institute for Automotive Engineering, University of Alabama, Tuscaloosa, USA; [b]Department of Mechanical Engineering, Bilecik Şeyh Edebali University, Bilecik, Turkey; [c]Department of Mechanical Engineering, Sakarya University, Sakarya, Turkey

ABSTRACT

This study investigates different biogas fuels' and operating conditions' effects on flame temperatures and emissions (CO, CO_2, NOx, and soot). Different calorific values (15.580, 17.880, 20.430, 23.080, and 26.230 MJ/kg) were obtained by changing methane content. Furthermore, various gas pressure (0.5, 1, 2, and 3 atm), excess air coefficient (1.4, 1.8, 2.5, and 4), and oxygen values (21, 23, 25, and 27%) were simulated for 8.6 kW thermal capacity furnace. Increasing the calorific value of biogas fuels, CO, NO_x, and soot emissions and flame length tend to increase, while CO_2 decreases. Increasing gas pressure, flame temperature, and CO_2, CO, and NO_x decrease, while soot emissions tend to increase. As a result of the decrease in the air excess coefficient from 4.0 to 1.4, there is a increase in the flame temperature, flame length, and soot, CO, CO_2, and NO_x emissions. On the other hand, oxygen content from 21% to 27% oppositely affected these parameters, excluding flame length.

ARTICLE HISTORY
Received 10 May 2023
Revised 2 May 2024
Accepted 21 May 2024

KEYWORDS
Oxygen-enrichment; excess air; soot; biogas flame; calorific value

Introduction

The fact that energy has become an essential need in our lives brings the concern of the current energy resources being exhausted over time. Therefore, evaluating renewable energy sources or alternative energy sources and investing in technologies will gain importance today and in the future. Biogas fuels as a biomass energy source can be shown among the prominent alternative fuels such as hydrogen, synthetic gas, and shale gas. Production differences such as pH value (Lehtomäki, Huttunen, and Rintala 2007), solid concentration (Deepanraj, Senthilkumar, and Ranjitha 2019; Liu and Lv 2016), period and temperature of fermentation, and the variety of raw materials (Tang et al. 2020) used to change the content of biogas, and therefore the flame characteristics of each produced biogas are not the same. In this case, a negative situation arises in front of the industrial and domestic use of biogas. Therefore, in literature, the combustion behavior of various biogas fuels has been considered in different combustion systems. Flame stability is an important issue in biogas combustion. Dai et al. (2012) investigated flame stability limits of biogas flame for reference test burner. They used six different test gases by changing CO_2 content between 30% to 45% for experimental study. Results showed that when the CO_2 fraction increased more than 45%, the mixture temperature decreased below 300°C and flame stability was almost lost. Furthermore, hydrogen addition with different CH_4 and CO_2 concentrations effects on flame stability on biogas non-premixed combustion in a co-flowing air stream was studied by Leung and Wierzba (2008). They found that introducing a small amount of hydrogen into biogas significantly enhanced the flame stability range. Colorado and McDonell (2018) investigated emissions and stability performance of different biogas and CO_2 mixtures at low-swirl

CONTACT Gokhan Coskun gcoskun@sakarya.edu.tr Department of Mechanical Engineering, Sakarya University, Esentepe Campus, Kemalpaşa District University Avenue, Serdivan, Sakarya 54050, Turkey

burner using experimental and CFD simulation methods. Özdemir, Yangaz, and Yilmaz (2021) investigated hydrogen-enriched fuels for methane, propane, LGP, Natural gas, and biogas combustion on premixed burner using CFD simulations. They observed the best improvement in biogas fuel, among other fuels. Their conclusion highlighted the promising potential of hydrogen-enriched biogas in premixed burners, especially when compared to the other tested fuels, considering both energy and exergy viewpoints. Devi, Sahoo, and Muthukumar (2023) experimentally realized the performance and emissions of a neand conventional burner with different equivalence ratios and biogas. With a new burner proposal, they have achieved a reduction of approximately 85% in CO emissions and a decrease of around 66% in NOx emissions. They also provided a 38% increase in thermal efficiency. Habib et al. (2021) investigated ultra-lean combustion experimentally with methane and biogas at different mixing ratios in a porous burner. According to the results obtained in the study, they have seen that methane and biogas can work at a low equivalence ratio. They have seen that flame rebound occurs after burning with a porous burner for a long time. They measured that biogas produces more CO emissions than methane. Alrbai et al. (2022). tried the use of biogas fuel in an HCCI engine. They investigated the effect of hydrogen sulfide in the content of biogas. They found that the separation and oxidation of sulfur in hydrogen sulfide causes undesirable emissions. A new chemical kinetic mechanism has been proposed by Alrbai, Al-Dahidi, and Abusorra (2021) for new components that will model biogas combustion and be different from other emissions. Charest, Gülder, and Groth (2014) studied the soot formation of biogas fuels under elevated pressures ranging from 1 to 20 atm in a laminar diffusion flame. It stated that dilution with CO_2 suppressed soot formation at all pressure. Fischer and Jiang (2015) studied the chemical kinetic aspects of the flame of biogas. They stated that in the case of stoichiometric and lean mixtures, increasing the initial CO2 concentration results in a reduction of NO production and an increase in CO production at elevated temperatures. However, for rich conditions, NO production is significantly lower and does not follow this pattern. Hoerlle and Pereira (2019) investigated the formation of soot and the effect of CO_2 addition under an oxygen-enriched atmosphere. They analyzed numerical data involving the addition of CO2 to fuel and oxidizer mixtures, maintaining an equivalent amount of CO2 within the reaction layer, using a series of laminar counterflow ethylene flames. They observed that the formation of species such as hydrocarbon radicals (C_2H, C_3H_3), C_2H_2, and A1, which are the building block types of PAH directly involved in the soot formation process, was suppressed by O_2. It was also found that adding CO_2 strongly affects the particle size distribution for existing flames. Hoerlle et al. (2020) compared the superposition WSGG radiation pattern with LBL spectral integration for a series of laminar unmixed counter-flow flames of ethylene burning with an oxygen-rich oxidizer. They combined soot generation with numerical and chemical solutions for both thermal radiation approaches. Systematically replacing N_2 with CO_2 in the fuel or oxidizer affects the role of thermal radiation, and the significance of radiation absorption in soot formation was investigated. As a result, they observed that a low strain rate occurs due to some non-negligible differences. Evaluation of the soot spectral radiation coefficient ($C_{K,s}$) revealed a significant effect on the soot fraction for low CO_2 addition levels. In their experimental study, Karataş and Gülder (2017) examined the impact of carbon dioxide and nitrogen dilution on the soot process of laminar ethylene diffusion flames under pressures of up to 20 atm. The investigation was conducted at a pressure of 10 atm within the nitrogen dilution range of 1:1 to 1:4. Within the pressure range of 1–15 atm, they observed that the tendency of the soot process to achieve maximum soot efficiency was notably lower when compared to carbon dioxide dilution. The rise in pressure led to a temperature decline, attributed to higher radiative heat loss. Additionally, the heat released from soot oxidation resulted in peak temperatures being detected around the flame tips. Liu et al. (2019) experimentally and numerically investigated the soot formation and exchange properties in premixed methane/ethylene-oxygen-argon flames.The experimental results demonstrated excellent congruence with the numerical simulation outcomes acquired through the validated SWOSMC technique. The results showed that while the coagulation rate increased in increasing ethylene flame, both condensation and nucleation rates increased in methane flame.In their study, Wei et al. (2020) employed experimental measurements of total CO, NO_x, and NO_2/NO_x ratios to calculate the

emission indexes (EI) of flame-wall interaction (FWI) in laminar mixed biogas-hydrogen flames. The results showed that with the addition of H_2, the EICO of the BG75-hydrogen flame steadily increased with the high reactivity of H_2, efficiently suppressing CO oxidation for the OH radical. Zhen et al. (2016) carried out an experimental study to investigate stoichiometric biogas-hydrogen blended fuel flames and investigated the combustion characteristics and heating performance of three hydrogen-enriched biogas. Observations from experiments have revealed that hydrogen has a favorable impact, whereas CO_2 has an adverse influence on flame stability. These findings indicate that, at elevated hydrogen fractions and increased CO_2 concentrations under constant Re and U conditions, the flame cone height experiences an extension. Furthermore, a polyhedral reaction flame cone was identified for stoichiometric flames with high hydrogen concentrations. Rocha, Quintino, and Fernandes (2020) carried out numerical and experimental studies of the chemiluminescent signals of OH, CH, C_2, and CO_2 for premixed laminar flames with hydrogen-enriched CH_4/CO_2/air. The results of OH/CH in the simulations showed the most consistent results with the experimental results. It is assumed that the OH/C_2, CH/C_2, and CO_2/CH results will reach good results with appropriate calibration. Hosseini and Vahid (Sarvestani et al. 2020) experimentally observed the performance of the flameless combustion chamber using biogas in a flameless combustion furnace under laboratory conditions. As a result, they showed that flameless combustion is one of the most suitable strategies and techniques for biogas. Bohlooli Arkhazloo et al. (2019) carried out an experimental and simulation study in a large-scale boiler. As a result of the study, they saw that the experimental and simulation studies gave very close results. Zhen, Leung, and Cheung (2013) experimentally studied the stability of a biogas diffusion flame and the effect of hydrogen addition on impingement heat transfer. By keeping the volumetric hydrogen content of the biogas between 5% and 10%, they revealed changes in the flame's appearance, stability, and heat transfer properties upon adding hydrogen to the biogas flame. The addition of hydrogen significantly increased the stability of the biogas flame. The initial 5% hydrogen addition was more efficient at improving stability than the other 5% hydrogen addition. In their research, Amar et al. (2018) examined the impacts of incorporating varying volumes of water vapor (ranging from 10% to 50%) into a mixture of biogas BG75 (consisting of 75% CH_4 and 25% CO_2) and hydrogen. As a result, it was shown that the combustion structure was very sensitive and variable to the water vapor and hydrogen mixture parameters. In their study, Nourbakhsh et al. (2018) conducted a thermodynamic assessment of syngas generation through the partial oxidation of biogas (POX). They utilized chemical equilibrium calculations employing the Gibbs free energy minimization method, with a focus on minimizing soot formation for (CH_4+CO_2) mixtures. Their findings highlighted the significant influence of process temperature in enhancing syngas production while diminishing soot formation. Moreover, the impact of pressure on syngas production efficiency was deemed impractical. It was determined that both hydrogen and carbon monoxide caused a decrease in soot formation. In their research, Sabnis and Aggarwal (2018) performed a simulation study to examine the emissions of NOx and soot in triple flames of n-heptane and methane, configured in a counter-jet arrangement. As a result of the simulation, it was observed that the benzene emission index and the soot emission decreased as the methane in the mixture increased. In order to achieve high thermal efficiency, a wide working range, and low pollutant emissions for steady combustion, modern technology focuses on lean premixed burners. Biogas combustion in a lean premixed burner was investigated by Fuzesi and Jozsa (2019) using a numerical analysis method. They used natural gas as a reference fuel while four biogas compositions including CO_2 and H_2 were tested. As a result, biogas fuel effectively burned in the designed test system. Another study was done by Habib et al. (2021) on ultra-lean combustion where methane and biogas were selected as test fuels studied experimentally in a porous burner. They found that the ultra-lean burner could work at equivalency ratios as low as 0.275 for both methane and biogas under steady conditions. Additionally, compared to methane, biogas produced more CO emissions. A new study on lean combustion where ammonia/biogas mixture used as fuel under-reacting swirl flow conditions was done by Mong et al (2023). They found that CO_2 addition has critical effects on ammonia/biogas mixture combustion characteristics.

They showed that the peak flame temperature was reduced by 150–300 K when the CO_2 mass fraction is increased to 40% in the premixed CH_4/NH_3 mixture as opposed to the zero CO_2 scenario.

Although many studies have focused on biogas flame and emission, it is understood that there are still deficiencies in the literature regarding soot and emission behavior under various calorific values, operating pressure, excess air, and oxygen-enriched combustion conditions. Besides, the previous studies handled biogas combustion around stochiometric combustion conditions; however, the combustion and emission performance of the biogas fuel on the lean mixture conditions are a few ones. In this study, detailed numerical data focused on pressure, excess air, and oxygen content effects on the combustion and emissions of five different biogas and methane fuels with different volumetric concentrations and characteristics under lean mixture conditions, which aren't encountered in the literature. The new trend in the combustion sector is to increase thermal efficiency and decreasing pollutant emissions at a wide range of operation simultaneously. therefore, lean mixture combustion draws attention to achieve this goal. Outrightly, this work is dedicated to completing this part of the literature. The present study aims to investigate the effects of different calorific values, pressure, excess air, and oxygen enrichment on sooting flames of biogas.

Numerical model

For modeling chemical reactions of biogas, non-premix (Moussa and Driss 2017) combustion with a Steady Diffusion Flamelet technique has been used in ANSYS Fluent 18.1 (ANSYS I. ANSYS FLUENT 2018). Gri-Mech 3.0 which including NO_x formation and reburn chemistry has been utilized for the chemical kinetic mechanism of the simulated fuels (Smith et al. n.d).

The following transport equation can be given to represent the governing equations, which encompass energy, momentum, mass, turbulent, and mixture fraction:

$$\frac{\partial \rho \varphi}{\partial t} + \frac{\partial}{\partial x_i}(\rho u_i \varphi) - \frac{\partial}{\partial x_i}\left(\Gamma_\phi \frac{\partial \varphi}{\partial x_i}\right) = S_\varphi \tag{1}$$

(Smith et al. n.d) In the context of the governing equations, where φ represents the scalar, Γ_ϕ stands for the diffusion coefficient, and S_φ denotes the source term (Yang et al. 2018).

In the current study, Reynolds number (Re) is approximately around 5000 for all fuels, indicating that the flow in the combustion chamber needs to be modeled as turbulent. The DO radiation model has been used for the heat transfer of radiation energy. For the modeling of turbulent flow, the Realizable k-ε turbulence model has been utilized (Cellek 2020b). Due to using boundary layer mesh, the Enhanced Wall Treatment near-wall model has been utilized (Cellek 2020a). Coupled and PRESTO! have been adapted for the pressure-velocity coupling scheme and pressure spatial discretization, respectively. Second-order upwind is chosen for governing equations (Kekec and Karyeyen 2020; Kekec and Karyeyen 2021) Moss and Brookes soot model is used for the soot formation prediction (Kekec and Karyeyen 2020). As mentioned in literature studies (Liu, Consalvi, and Nmira 2023) accurately modeling of soot and radiation coupling laminar and turbulent flames is important. For the current study, Moss Brookes soot model presented good estimation among others, including one-step soot model, method of moments model, and Moss Brookes model, possibly due to lean mixture condition. User-correlation was selected for the soot precursor for CH_4 fuel to calculate soot emissions. For precursor correlation, pieces-polynomial profile with three coefficients as 3.797e-06, −0.00192 and 0.05277 applied to the soot model. Fenimore-Jones model is employed for soot oxidation. Instantaneous OH species are used for the model parameters. The 2D axisymmetric model view and mesh structure of the combustion chamber with a length of 1.25 m and a diameter of 0.155 m is shown in Figure 1. The mass flow boundary defines the air and fuel inlet, while the pressure outlet is defined for the outlet boundary condition. The temperature of air and fuel are the same as 290 K, respectively. The geometry of the combustion chamber is cylindric; thus, the axisymmetric boundary condition is

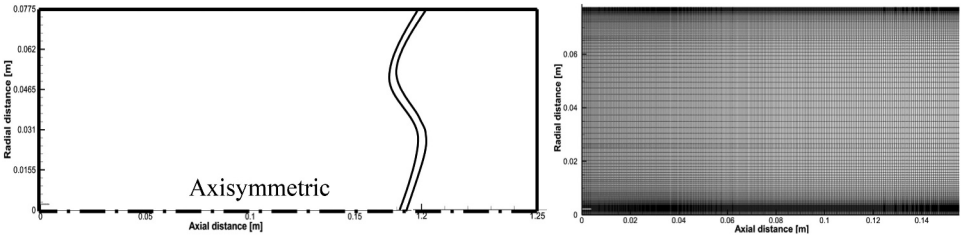

Figure 1. Geometrical model and boundary layer mesh generation for the computational zone.

Table 1. Simulated fuels, mole fractions and operating conditions.

Components	Biogas 1	Biogas 2	Biogas 3	Biogas 4	Biogas 5	Methane
CH_4	0.55	0.60	0.65	0.70	0.75	1
O_2	0.0037	0.005	0.007	0.005	0.005	-
CO_2	0.431	0.38	0.33	0.2935	0.2435	-
N_2	0.0153	0.015	0.013	0.0015	0.0015	-
C/H	0.25	0.25	0.25	0.25	0.25	0.25
MW [kg/kgmol]	28.338	26.929	25.539	24.349	22.950	16.042
LHV [MJ/kg]	15.580	17.880	20.430	23.080	26.230	50.000
Pressure [atm]	1–3	1	1	1	1	1–3
T_{air} *and* T_{fuel} *[K]*	290	290	290	290	290	290
$\dot{m}_a$ *[kg/s]*	0.01173004	0.01172435	0.01170686	0.011726	0.011731	0.01180
$\dot{m}_f$ *[kg/s]*	0.000552	0.0004809843	0.0004209496	0.0003726	0.0003278	0.000172

utilized for the numerical simulation. The wall boundary condition is used for the chamber non-interior parts, such as walls. The main fuel enters the chamber through a circular section with a diameter of 4.07 mm through the axial center. While pilot fuel enters the chamber within 0.16 mm diameter nozzles. Pilot fuel is sent to the chamber through a 0.16 mm diameter nozzle. The total of fuel mass flow rate at the entrance is 0.000552 kg/s. Air is introduced to the chamber through the rest of the radial distance as 0.01173004 kg/s. Therefore, this study is conducted under lean mixture condition that the equivalence ratio is 0.25; in other words, the excess air is 4. Meanwhile, the axial distance results were obtained from the axisymmetric line of the 2D model.

Fuel properties

Although synthetic gases draw the attention of researchers due to the increment in energy demean (Alabaş et al. 2021; Yilmaz and Ilbas 2008; Yilmaz et al. 2017, 2020), methane is more easily accessible. It has a cleaner combustion nature with a lower carbon/hydrogen ratio and causes less CO_2 and HC emissions (Şanlı, Yılmaz, and Gümüş 2021). On the other hand, biogas fuels contain high amounts of carbon dioxide by volume. Hence, the calorific energy value of Biogas fuels is lower than other conventional gaseous fuels such as pure methane, natural gas, propane, and hydrogen. The basic disadvantage of biogas is their weak flame due to their low heating values (calorific value) (Zouagri et al. 2020). Therefore, their calorific value can be enhanced by fuel H_2-blending fuels (Mameri and Tabet 2016). Component and volumetric percentages of biogas 1, Biogas 2, and Biogas 3 fuels have been obtained from the study published by İlbaş, Şahin, and Karyeyen (2018). The fuel properties of Biogas 4 and Biogas 5 are obtained from the Unitrove-engineering tools (Unitrove 2021). The numerical simulations of biogas fuels have been carried out at the same thermal capacity of 8.6 kW under lean conditions. Utilizing lean combustion results in minimal formation of pollutant species, along with an unstable flame, which holds significant importance in industrial applications Amar et al. 2018.

The components, percentages, lower calorific values, and other properties of the fuels handled in this study are presented in Table 1.

Results and discussion

Verification and validation of the numerical model

In this study, before the target fuels' serial analysis, the combustion chamber's grid generation was investigated with five different mesh numbers to display the mesh independence for verification, as shown in Figure 2(a). It is found that the flame temperature and mean mixture fraction data obtained with a low mesh number (36552) show different tendencies, while the others show a similar trend. Although 56,760 elements show sufficient results, 122,710 elements were selected for better resolution of the computational domain in the study. Furthermore simulations employing 122,710 elements yield more satisfactory NOx results compared to those with 56,760 cells, with a percentage error of 5.46% as given in Table 2. This discrepancy underscores the necessity of conducting the study with 122,710 cells rather than 56,760 cells.

On the other hand, the numerical combustion of methane gas has been validated with reference experimental data published by Brookes and Moss (1999). Flame temperature, mean mixture fraction, and soot volume fraction prediction data have been compared with experimental ones, as shown in

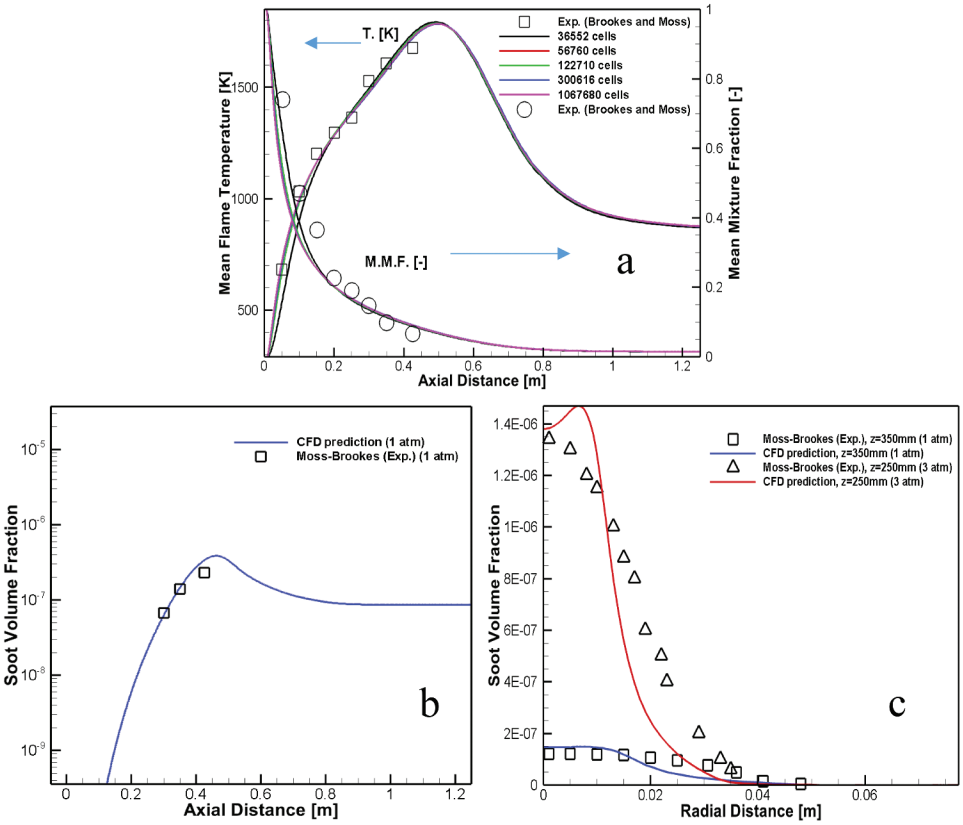

Figure 2. Mesh independence study of the numerical model for verification (a) and comparison of experimental and numerical results for validation for CH_4 fuel (b,c).

Table 2. Simulation results and solution times of different element numbers.

Element numbers	NOx emission at the outlet, ppm	Percent Error, %	Solution Time (minutes)
36552	*5.184*	*7.46*	*5*
56760	*5.296*	*5.46*	*19*
122710	*5.602*	-	*53*

Figure 2(b,c). Unlike others, the soot volume fraction of the numerical results is given both on the axial and radial lines for various operational pressures. The results show that flame temperature, mean mixture fraction, and soot volume fraction results on the axial lines agree with the experimental results. Furthermore, the soot volume fractions prediction of the numerical results on the radial lines at two locations are close to experimental results under 1 and 3 atm. Therefore, it is considered that validation is provided considering the results obtained from the flame temperature, mean mixture fraction, and soot formation on the axial and radial direction numerical model.

Effects of calorific value on combustion and emission

Methane and biogas fuels' combustion and emission behavior with five different calorific values have been investigated. When mass fraction variations of methane are examined in Figure 3(a), methane in biogas fuels is consumed at the axial distance of about 0.3 m of the combustion chamber. Mass ratios change of 100% methane show a different trend from biogases and continue up to 0.55 m in length. No unburned methane concentration is observed in the later parts of the combustion chamber. When curves of average flame temperature variation with axial distance are examined in Figure 3(b), it is seen that the maximum mean flame temperature value varies between 1700–1800 K. Mean flame temperatures of Biogas 1, Biogas 2, and Biogas 3, which have low calorific values at a distance of 0.3 m in the axial direction, are around 1800 K. Biogas with low calorific value has high flame temperature because a higher amount of CH_4 fuel reacts in the form of shorter flame. It is seen that the lowest maximum flame temperature is obtained in Biogas 5 and methane gas. In addition, mean flame temperature tends to decrease with increasing calorific value in biogas mixtures and axial distances corresponding to the peak temperature increase. The axial distance corresponding to the peak point is around 0.5 m for pure methane gas.

Figure 3(c-f) shows the variation of CO_2, CO, soot volume fraction, and NO_x emissions in the combustion chamber with axial distance. The distribution of CO_2 emissions during the combustion of fuels with different calorific values is shown in Figure 3(c). Since biogas mixtures contain CO_2, CO_2 is initially present at the entrance to the combustion chamber, depending on its mole ratios. Due to combustion, its CO_2 has decreased since its introduction. Afterward, the concentration in the axis of the combustion chamber (0.4–0.9 m) decreased and constantly left the combustion chamber in a constant manner, as the CO_2 released in the reaction zone met with the combination of C and O_2 and increased slightly, and then other species (H_2O, CO, O_2, N_2, NO_x) were also released. In pure methane, since there was no CO_2 at the beginning, CO_2 increased from zero due to the reaction. For biogas mixtures, CO_2 decreased at an axial distance of 0.2 m and then increased again, reaching its maximum value of around 0.35 m. After the axial distance of 0.35 m, the CO_2 decreased around 5–6% and was stabilized by increasing the axial distance for all biogas mixtures. Methane gas showed a two-stage increase and reached an 8% CO_2 emission value around 0.55 m and, decreased with increasing axial distance and stabilized at 4%. With the increase in calorific value, the amount of CO_2 in the fuel and the CO_2 emission emitted at the combustion chamber exit decrease.

The distribution of CO emissions during the combustion of fuels with different calorific values is shown in Figure 3(d). Higher CO emission was revealed with increasing calorific value. The maximum amount of CO formed from Biogas 5 and methane is lower in ppm value compared to other biogas mixtures. The released CO emissions generally peaked (90000–100000 ppm) in the fuel-rich regions (around 0–0.2 m axial distance). Afterward, CO_2 conversion increased with the presence of oxygen, and sharp decreases were observed in CO emissions. Pure methane has reached a maximum value of 82,000 ppm at 0.35 m axial distance.

The distribution of Soot Volume Fraction during the combustion of fuels with different calorific values is shown in Figure 3(e). Soot formation started at an axial distance of 0.2 m, and the maximum point occurred around 0.42 m axial distance for all cases. The soot volume fraction was a maximum value minimum $1.2 \times 10–7$ for the Biogas 1 mixture. The highest soot formation was $4.3 \times 10–7$ in the Biogas 4 mixture. As can be seen from the figure, soot formation was less in the fuel-rich region and

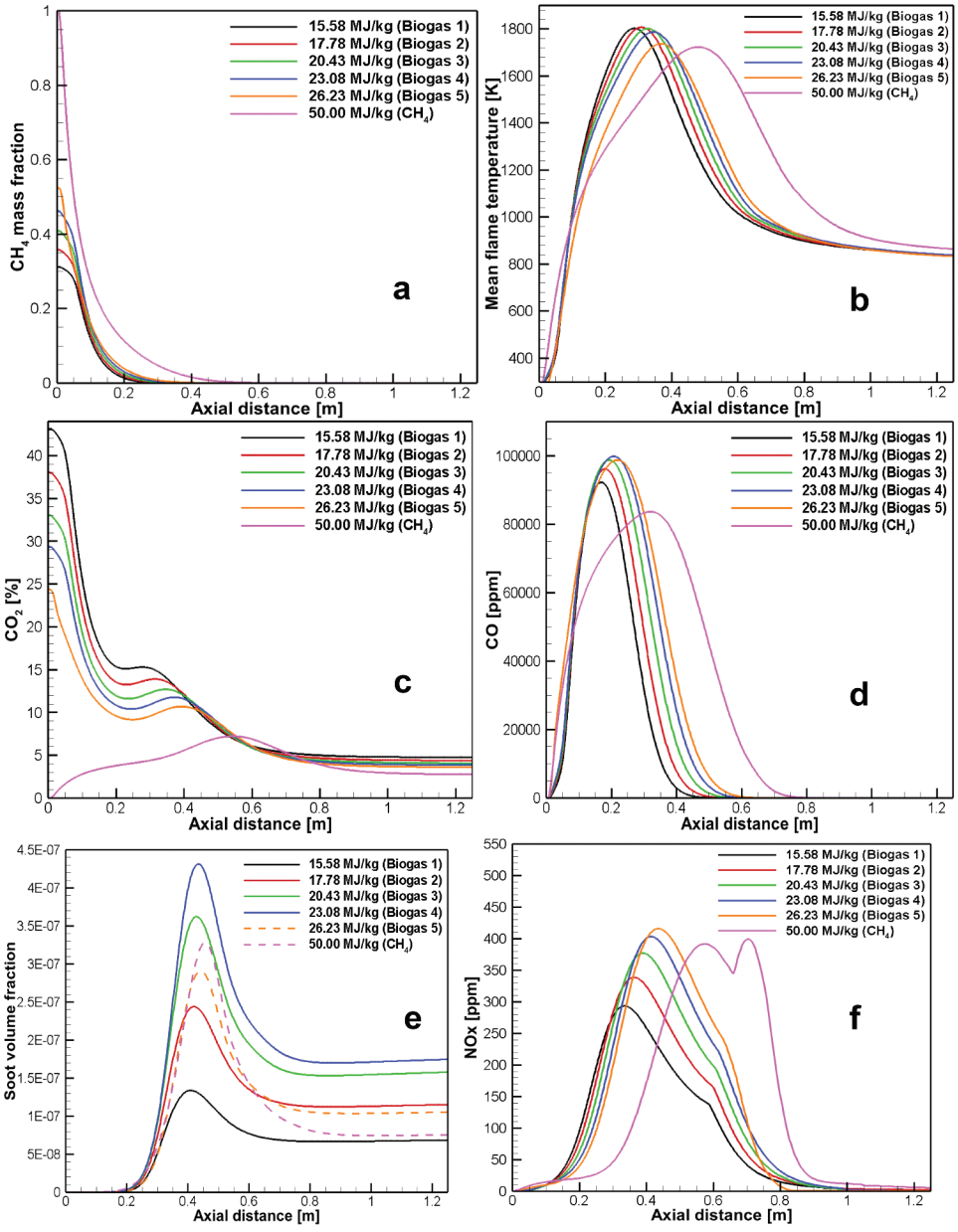

Figure 3. Emissions with changing axial distance for different calorific value.

peaked under high temperatures in the region where the combustion reaction developed (0.2 m-0.4 m axial distance). Soot formation also increased with increasing calorific value, similar to CO emissions. However, the maximum soot formation value of Biogas 5 and methane occurred between biogas 2 and 3. The amount of carbon-derived fuel components in biogas determines the soot amount by affecting the unburned carbon composition.

The distribution of NO_x emissions during the combustion of fuels with different calorific values is shown in Figure 3(f). Biogas mixtures maximum value of NO_x increased in the range of 290 ppm-416 ppm according to increasing calorific value starting from 0.32 m axial distance toward 0.48 m axial distance. Flame temperature and unburned hydrocarbon intermediates, such as OH and HC,

significantly affect NO_x formations. The amount of NO_x increases with the prompt NO_x mechanism in the fuel-rich regions from the entrance region. In the flame region and in the regions where the temperature is high, NO_x emissions generally originate from thermal NO_x. Low levels of NO_x emission were observed in the inlet region for biogas mixtures. NO_x emission is seen to spread at a high level at an axial distance of 0.3–0.5 m. Biogas flames coincide with the region where the flame temperature is maximum. Two different peak values occur in methane gas. A high level of NO_x formation is observed with the effect of radicals such as intermediate products OH and HC in the combustion zone, with the first peak value around 0.5–0.65 m. On the other hand, at the second peak value, it can be shown that N and O atoms in the reaction zone combine to trigger NO_x formation under high temperatures. In Figure 4(c), it is seen that the NO_x concentration reached its maximum value in two successive areas.

Temperature, soot volume fraction, and NO_x emission distributions in the axial plane of the combustion chamber are compared for biogas mixtures and methane fuels with different calorific values in Figure 4. The effect of increasing calorific value on temperature distribution can be seen in Figure 4(a). It has been observed that the flame length of biogas mixtures is generally short, and the flame length increases with increasing calorific value. It is seen that flame lengths of biogas fuels vary between a minimum of 0.45 m and a maximum of 0.55 m. Since the calorific value of

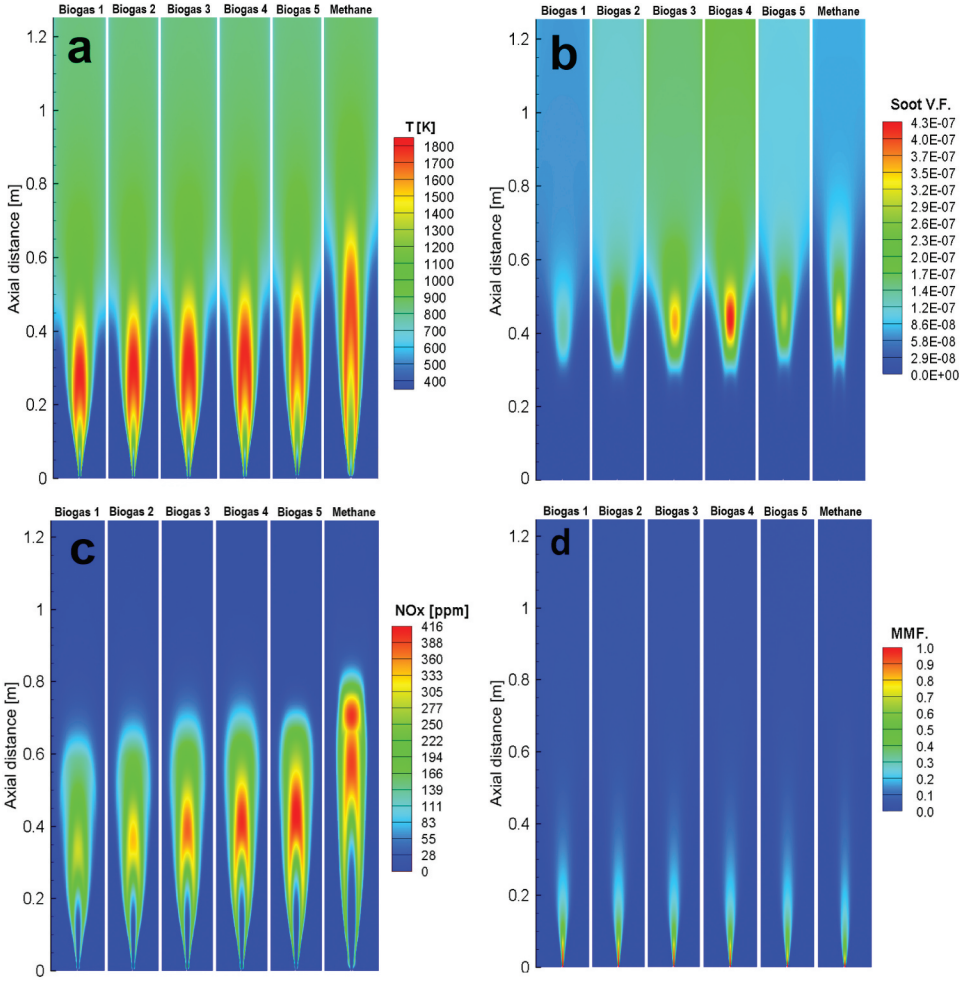

Figure 4. Temperature, Soot Volume Fraction, NO_x and Mean Mixture Fraction distribution with changing calorific value image inside combustion chamber.

methane gas is high, the methane flame length is about 0.75 m. The middle part of methane and biogas flames reaches a temperature of around 1800 K. The temperature continued in the range of 900–1000 K toward the end of the combustion chamber for each gas. The effect of increasing calorific value on soot volume fraction distribution can be seen in Figure 4(b) Similar to the soot volume fraction graph (Figure 4(c)), a minimum level of soot formation was observed in the Biogas 1 mixture in the soot volume fraction image. Soot emissions in biogas fuels increased gradually for Biogas 1, Biogas 2, and Biogas 3. The amount of soot decreased when the CH_4 mass fraction increased by 75% or more (Biogas 4, Biogas 5, and pure methane). It is seen that soot formation is maximum at the end of the combustion reaction zone and in the region where the temperature is high, where unburned hydrocarbons cannot be oxidized. It is seen that the regions where the soot formations begin, and peak are close to each other in terms of axial distances (0.3 m-0.5 m).

NO_x emission contours on the combustion chamber axis plane are shown in Figure 4(c). While minimum NO_x emission was observed in Biogas fuel with low calorific value, NO_x emission from biogas and methane fuels increased with increasing calorific value. It is seen that NO_x emissions released are proportional to reaction region lengths. Due to locally unburned hydrocarbons in the contact line of fuel and air at the inlet combustion chamber, the prompt NOx mechanism causes high levels of NO formation. At the entrance of the combustion chamber, this ratio is low in terms of NO_x formation. NO_x emission is quite high in the reaction region and the region where temperature peaks. In this region, NO emissions which were previously formed by the prompt NOx mechanism, and N_2 molecules are oxidized and form NO_2 with the thermal NO_x mechanism. There are high concentrations of NO_2 emissions toward the end of the combustion chamber. NO_2 emissions are intensely converted to N_2 and NO, causing a decrease in the amount of NO and N_2 molecule species. According to the temperature image, NO_x was formed in the regions where the temperature exceeded 900 K. NO_x increased in the regions where temperature distribution increased toward the flame.

The mean mixture fraction distribution of biogas and methane fuels are represented in the Figure 4(d). It is observed that the amount of fuel in the mean mixture is quite high near the entrance, then decreases gradually through the axial distance. Almost no fuel left toward the exit of the combustion chamber for each fuel. On the other hand, the fuel spreads much more in both radial and axial directions for biogas fuels that include relatively high amount of CO_2 percentage whereas it spreads more in the axial direction. Thus, these distribution differences affect the reaction zone location, fuel temperatures, intermediates, and combustion products in the chamber, as seen in Figure 4(a-c). The NO_x emission is quite sensible to flame temperature and the amount of intermediate species; thus, NO_x distribution patterns seem to differ, as shown in Figure 4(c)."

Effects of pressure on combustion and emission

The pressure, which affects combustion and emission, has been studied parametrically. For the Biogas 1 mixture with the lowest calorific value, combustion was carried out at pressure values of 0.5, 1, 2, and 3 atm. Figure 5 shows the variation of mean mixture fraction (Figure 5(a)) and mean flame temperature (Figure 5(b)) with axial distance under different gas pressures for the Biogas 1 fuel mixture. It is seen in the mean mixture fraction graph that there is more fuel mixture in the combustion reaction zone under high pressure. At the same time, it is seen that the mean mixture fraction reaches the point of depletion at a shorter distance in the axial direction with increasing pressure. The early gas consumption caused a decrease in mean flame temperature and maximum point value. It is also seen that flame length and temperature decrease with increasing pressure. The variation of CO_2 emission with axial distance for different pressures is shown in Figure 5(c). Similar situations were observed between the mean mixture fraction and CO_2 emission. Higher CO_2 emissions were obtained due to more fuel with increasing pressure in the same axial distance. As fuel consumption reached the point of depletion, CO_2 levels decreased with increasing axial distance. In general, due to the CO_2 gas

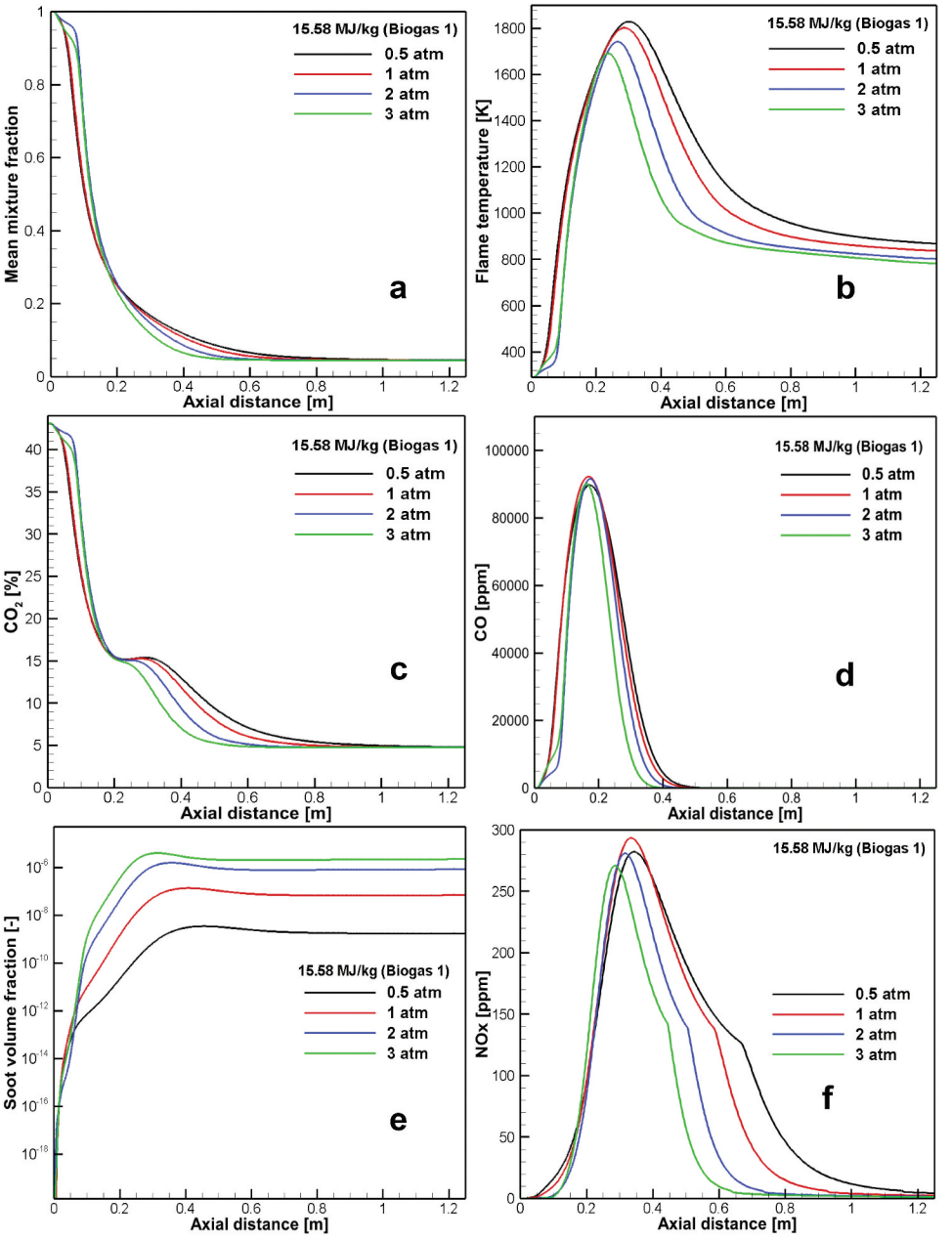

Figure 5. Mass fractions, flame temperatures and emission distribution of biogas fuel under various pressure.

in the biogas fuel mixture, the CO_2 concentration, which starts at around 45%, quickly drops to 15% up to an axial distance of 0.2 m. CO_2 emission was fixed at around 5% at each gas pressure toward the combustion chamber outlet.

Variations of CO emission with axial distance for different pressures are shown in Figure 5(d). It is seen that CO emission emitted in combustion reaction under high pressure is shifted according to axial distance. In addition, it is seen that CO_2 conversion of CO emissions caused by short flame length is completed earlier in the presence of oxygen. CO levels reach approximately 9200 ppm at 0.2 m axial distance for all gas pressures. It also reaches 0 ppm at 0.45 m axial distance.

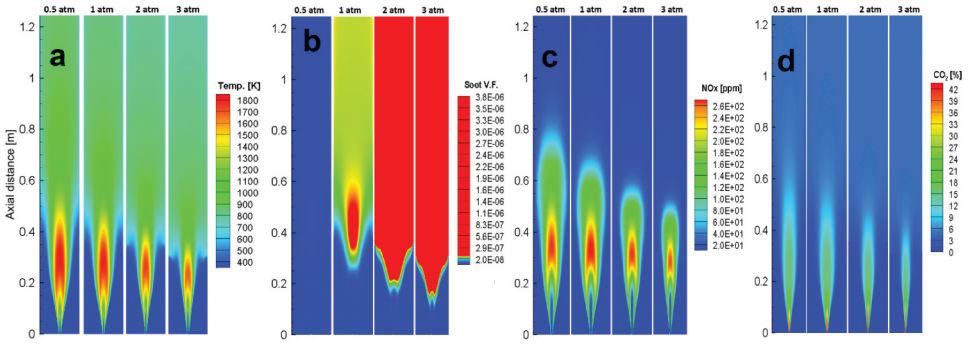

Figure 6. Temperature (a), Soot Volume Fraction (b), NO_x (c) and CO_2 (d) distribution with changing pressure image inside combustion chamber.

Variations of soot emission with axial distance for different pressures are shown in Figure 5(e) high gas pressure significantly increased the formation of soot. While soot was formed 10^{-6} values for 3 atm gas pressure at 0.3 m axial distance, about 10^{-8} levels of soot were formed at 1 atm pressure. Soot peaks were slightly shifted forward with increasing pressure. Variations of NO_x emission with axial distance for different pressures are shown in Figure 5(f). As with CO emission, high gas pressure caused late-onset and early depletion of NO_x formation. Contrary to soot formation, a decreasing trend was observed in NO_x emissions when the combustion chamber operating pressure was increased. The high gas pressure caused axial distances corresponding to maximum NO_x values to decrease. This is due to the shortening of flame lengths.

When the variation images of the temperature distribution (Figure 6(a)) according to gas pressure are examined, it is seen that the flame length and temperature decrease with increasing gas pressure. This is because fuel consumption under high pressure is depleted in a short axial distance. The flame length was measured as 0.3 m for 3 atm gas pressure and 0.45 m for 0.5 atm gas pressure. While temperatures in the flame regions are around 1800 K, it is seen that the temperatures are around 900 K toward end of the combustion chamber. Figure 6(b) shows that a very low amount of soot is formed for 0.5 atm pressure. A situation similar to the Soot formation graph has been observed. It was observed that soot formation increased significantly with increasing pressure. If the same scale was used for comparison, the difference between the minimum and maximum was very large. On the color scale, the blue color represents the lowest value. The red color indicates the maximum level. A completely blue color was formed at 0.5 atm pressure. That is, the lowest level of institution was formed among all cases. Since the value of 10^{-7} and above is red on the color scale, it was seen as completely red at 2 and 3 atm pressures. When the NO_x emission image in Figure 6(c) is examined, NO_x emission is seen in regions around 900 K. NO_x emission increased in regions where the temperature increased toward the flame. NO_x emission maximum value and corresponding axial distances change with flame length and reaction zone. As can be seen from the variation with NO_x axial distance, there is higher NO_x emission at low pressures. The NO emissions are diminished at high pressure by recombination reactions that disable chain carrier radicals (Mameri et al. 2019). When the distribution of CO_2 emissions in Figure 6(d) is examined, since the amount of CO_2 in the fuel composition is high, there is a high CO_2 concentration at the inlet combustion chamber, while a high concentration is diluted in the reaction zone. A lower level is noticeable toward the end of the combustion chamber. Lower concentration is observed toward the end of the combustion chamber with increasing pressure. It is seen that CO_2 is released throughout the flame.

Effects of excess air and oxygen enrichment on combustion and emission

In this section, in order to examine the combustion properties of biogas fuel, the effect of excess air on emission and soot formation has been investigated by changing the excess air coefficient of 1.4, 1.8,

2.5, and 4, respectively. Besides, for the case where the excess air coefficient is 4, the oxygen enrichment percentage is gradually increased from 21% to 27% to reveal the effect of oxygen enrichment on biogas combustion performance.

The effect of the excess air coefficient on the flame temperature of biogas fuel is shown in Figure 7(a). It is observed that the flame peak temperature decreases with increasing air excess coefficient. Similarly, the combustion chamber outlet temperature decreases with increasing air excess coefficient. When the effects of oxygen-enriched combustion are examined in Figure 7(b), it is seen that the flame peak temperature, as well as flue gas temperature increases with the increasing oxygen percentage. Increasing the oxygen percentage from 21% to 27% has increased the flame peak and flue gas temperature by approximately 200 K and 120 K, respectively.

When the soot formation graph (Figure 7(c)) is examined along the combustion chamber axis, the increasing air excess coefficient decreases the amount of soot formed. It is seen that the formation of soot is completed when the air excess coefficient is 4. However, it continues to increase toward the exit for other excess air coefficients. It appears that the soot formation starts to increase significantly when the flame temperature is in the range of 1400–1600K. In oxygen-enriched combustion, it has been observed that the increased amount of oxygen encourages the formation of soot and increases it gradually as shown in Figure 7(d).

It has been observed that the increase in the excess air coefficient reduces the amount of carbon dioxide in the combustion chamber axis toward the combustion chamber outlet, as shown in Figure 8(a). This situation can be explained by the fact that fuel residues under high flame temperature inside the chamber react to form CO_2. CO_2 formation has been encouraged with lower excess air coefficients. In oxygen-

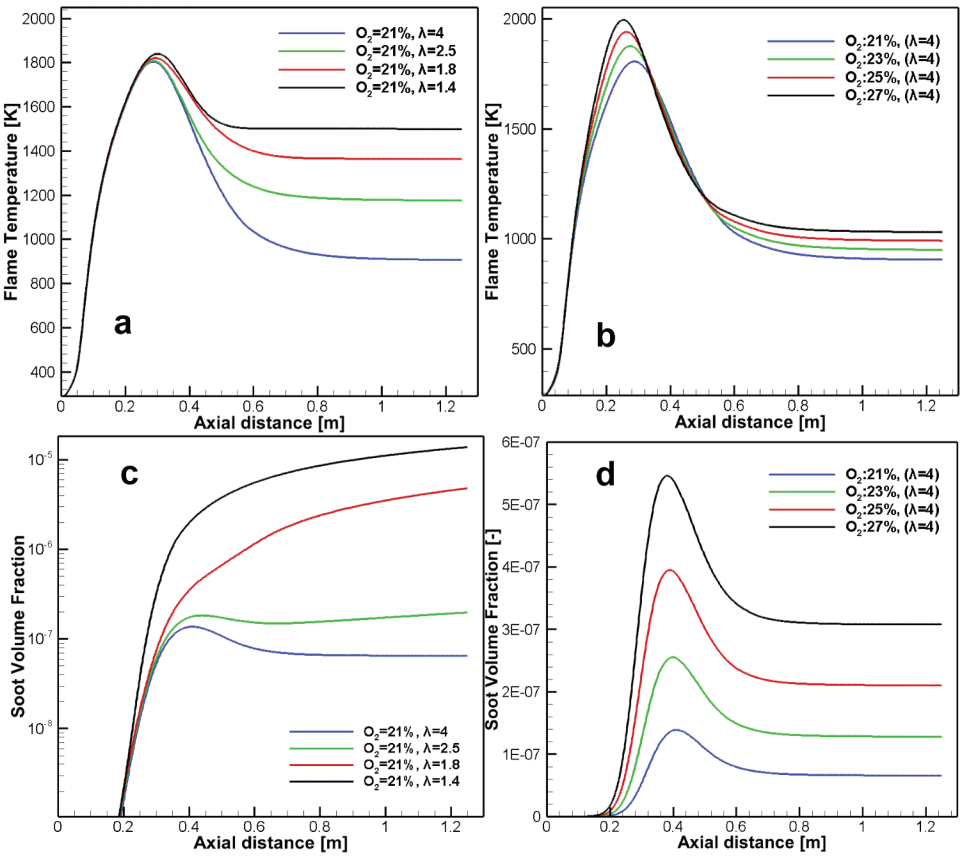

Figure 7. Variation of flame temperatures and soot formation of biogas under various excess air and oxygen enrichment conditions.

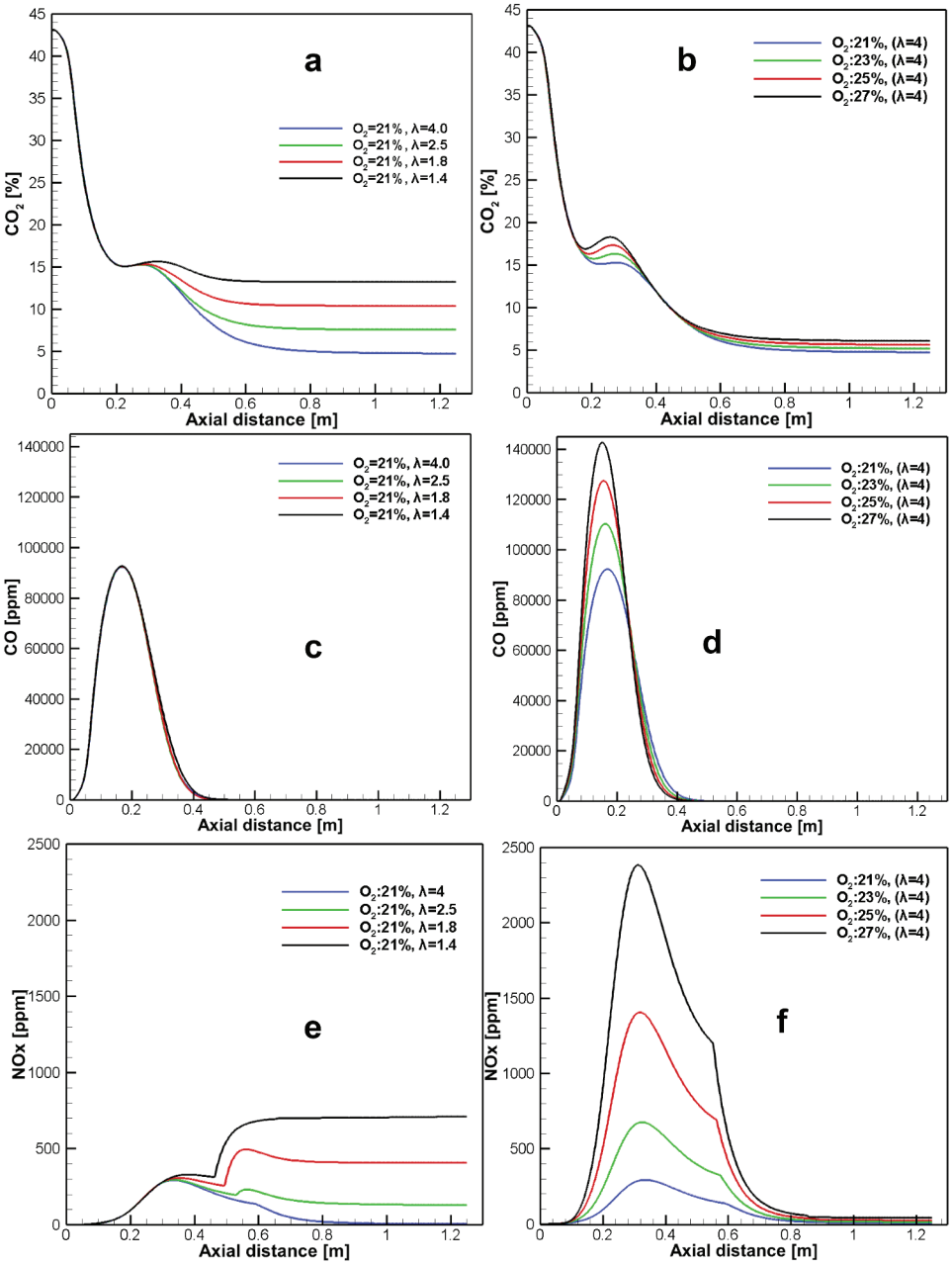

Figure 8. Variation of pollutant emission under excess air and oxygen enrichment.

enriched combustion, the formation of CO_2 increases with the increasing oxygen percentage, as presented in Figure 8(b). However, the amount of increase in CO_2 formation is relatively lower than in the cases with excess air coefficient.

As for CO emissions, as shown in Figure 8(c,d), the effect of increasing air excess coefficient on CO emissions is very limited. On the other hand, although the CO level formed in the combustion chamber increases significantly with increasing oxygen percentage, CO is depleted by participating in the reaction chain after a short distance to form CO_2.

Figure 8(e-f) shows the effect of excess air and oxygen enrichment variation on NO_x emissions. NO_x formations have decreased with the effect of flame temperatures decreasing, as shown in Figure 8(e). The maximum point of NO_x formation occurred in the range of axial distance 0.30–0.55 m. The maximum level of NO_x is about 600 ppm for $\lambda = 1.4$, while it is 293 ppm for $\lambda = 4$. Since the excess air coefficient reduction increases the flame temperatures toward the combustion chamber exit, this increases NO_x in the combustion chamber exit region. When the effect of oxygen-enriched air on NO_x emission is examined by keeping λ constant in Figure 8(f), the maximum NO_x formation occurred at 0.35 m axial distance for all cases. It has also been observed that the amount of NO_x released on the axial line increases gradually with increasing oxygen enrichment. Although NO_x emission levels in the outlet region decrease, the amount of emissions emitted at the outlet also increases slightly with oxygen enrichment. In the flame enriched with oxygen, the maximum levels of NO_x measured in the combustion chamber are 2400, 1400, 680, and 293 ppm for 27%, 25%, 23%, and 21% cases, respectively.

The effect of changing air excess ratio (λ) on mean flame temperature, soot volume fraction, and NO_x can be seen in Figure 9. The effect of decreasing λ value on mean flame temperature distribution can be seen in Figure 9(a). Decreasing λ value increases mean flame temperatures. The peak flame temperatures measured on the center plane are 1804, 1808, 1820, and 1840 K for $\lambda = 4$, 2.5, 1.8, and 1.4, respectively. The combustion chamber temperature has reached its maximum value of 1550 K from 0.5 m axial distance at $\lambda = 1.4$, and it is around 950 K for $\lambda = 4$.

The effect of decreasing λ value on soot volume fraction distribution can be seen in Figure 9(b).

Since the color scale is in the range of 10^{-6}-1.7×10^{-5}, it has been observed that it is almost completely blue (minimum level) for $\lambda = 4$ and $\lambda = 2.5$. On the other hand, due to the color scale, the opposite effect is seen completely red in $\lambda = 1.8$ and $\lambda = 1.4$. In other words, the amount of soot increases significantly with the decreasing λ. The reason for this situation is an increase in the amount of unburned carbon at low λ.

The effect of changing air excess ratio (λ) on mean flame temperature, soot volume fraction, and NO_x can be seen in Figure 9. The effect of decreasing λ value on mean flame temperature distribution can be seen in When the NO_x image is examined, the amount of NO_x released gradually decreases with the increase in λ as shown in Figure 9(c). This is beneficial in terms of showing the advantage of performing combustion at a high excess air coefficient. Low NO_x is emitted in the reaction zone in the inlet parts, while a high amount of NO_x is emitted in the high-temperature zone. The amount of NO_x to be thrown into the environment is the value read at the exit of the combustion chamber.

The effect of changing oxygen amount in the air on mean flame temperature, soot volume fraction, and NO_x can be seen in Figure 10. The effect of increasing oxygen amount in the air on mean flame temperature distribution can be seen in Figure 10(a). Mean flame temperature increased with increasing oxygen content. The mean flame temperature reached its maximum of 2000 K in the 0.3–0.35 m axial distance range.

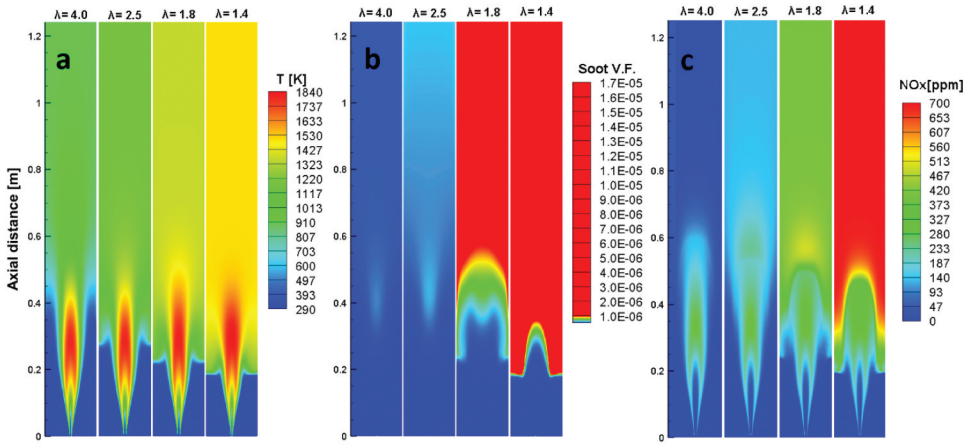

Figure 9. Temperature (a), Soot Volume Fraction (b) and NO_x (c) with changing excess air coefficients image.

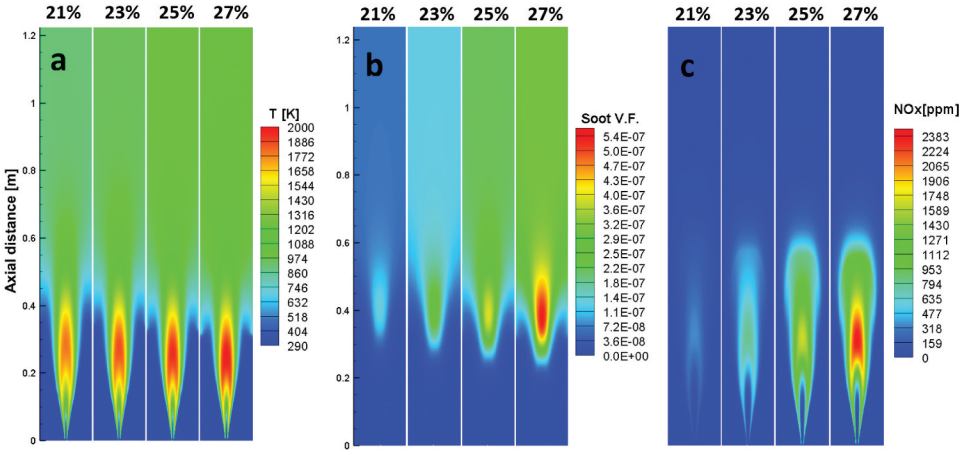

Figure 10. Temperature (a), Soot Volume Fraction (b) and NO_x (c) with changing oxygen percentages image.

The effect of increasing oxygen amount in the air on soot volume fraction is seen in Figure 10(b) soot volume fraction increased with increasing oxygen amount. Regardless of the amount of oxygen, soot volume fraction reached its maximum value in four cases at 0.4 m axial distance, slightly beyond the maximum value of mean flame temperature.

As a result of oxygen enrichment, the nitrogen in the air reacts with more oxygen to form more NO_x, especially around the reaction zone, as shown in Figure 10(c). The highest NO_x amount comes out as a result of the highest oxygen enrichment. Outside the reaction zone, NO_x has gradually reduced for all cases due to the reaction of 2NO and N_2 to $2N_2O$ species.

Conclusion

In this study, the numerical model validated with temperature, mean mixture fraction, and soot volume fraction data published by Brookes and Moss (1999) for methane combustion, the combustion and emissions of biogas fuels under different calorific values, operational pressure, excess air, and oxygen-enriched combustion conditions have been investigated. The findings obtained in this study can be listed as follows:

- With the increase in calorific value, especially CO_2 emission decreased toward the end of the combustion chamber. Especially with increasing calorific value CO, NO_x emissions, and the flame length have increased. The soot volume fraction released from biogas fuels increases until the calorific value reaches 23.08 MJ/kg, then decreases with increased calorific values. It was understood that when the calorific value of the fuel was increased from 15.58 Mj/kg (biogas 1) to 50 MJ/kg (methane), the flame length increased by approximately 50%. There was a 3.6 times difference between the two mixtures in terms of soot volume, with biogas 4 having the largest soot volume and biogas 1 having the lowest soot volume. It has been observed that the highest CO_2 value occurs in Biogas 1, and the lowest CO_2 value occurs in methane, with a difference of approximately 40% between them. This result has emerged because the CO_2 ratio in the Biogas 1 mixture is at the highest value. It has been observed that the CO emission resulting from the combustion of Biogas 1 is 9% higher in the combustion of methane, while Biogas 5 fuel causes 10% more CO emissions than Biogas 1. It is understood that Biogas 5 and methane combustion produce the highest NO_x emissions, which are about 50% greater than biogas 1.
- When the effect of different pressures with Biogas 1 is examined, no significant change was observed in CO and CO_2 emissions with the increase in pressure. By subtracting the gas pressure from 0.5 to 3

atm, an approximately 4-fold increase was observed. It was observed that there was a 6% decrease in flame temperature and a 5% decrease in NO_x emissions with the increase in pressure.

- As a result of the numerical analysis, increasing excess air coefficient decreases the flame and flue gas temperatures, CO_2, NO_x, and soot emission in the combustion chamber, while increasing oxygen percentage increases the flame and flue gas temperatures, CO_2, NO_x, and soot emission. On the other hand, there is a slight decrease in CO emission levels with an increase in excess air coefficient. With an increase in the oxygen percentage, the CO level through the flame in the combustion chamber has increased and earlier turned into CO_2 emission in the reaction chain. The study investigated the effect of the excess air coefficient for biogas 1. It should be noted that different results will occur in combustion performance and emission values with the change of air excess coefficient in various calorific value biogas fuels.

In line with the results obtained from the study, it was seen that the effect of different gas inlet pressures, calorific values, and excess air coefficient values on burner combustion is significant. As a continuation of this study or in light of this study, it has been seen that using biogas with low gas inlet pressure and high excess air coefficient can provide an ideal combustion, especially for using biogas in burners. Combustion efficiency can be increased by optimizing the accuracy of such simulation studies instead of experimental study costs and by optimizing simulation studies for different burners and various gas combinations in future studies. Existing simulation studies will guide future experimental studies.

Disclosure statement

No potential conflict of interest was reported by the author(s).

Funding

The author is grateful for using the computing resources provided by the National Center for High-Performance Computing of Turkey (UHEM, UYBHM) under grant number [1010322021].

Notes on contributors

Mehmet Salih Cellek joined the Institute for Automotive Engineering Department at University of Alabama. He received his BE (2010) and MSc (2013) from Sakarya University and PhD (2017) from Yildiz Technical University. His doctoral research was on the investigation of combustion emissions in industrial burner-boiler systems. He has interest in combustion, alternative fuels, and combustion modelling using CFD.

Usame Demir joined the Mechanical Engineering Department at Bilecik Şeyh Edebali University. He received his BE (2010), MSc (2013) and PhD (2017) from Sakarya University. His doctoral research was in Electromechanic variable valve timing for internal combustion engine modelling usingcomputational fluid dynamics (CFD). He has interest in the following research areas are internal combustion engines, HCCI engine, alternative fuels, combustion modelling using SRM and CFD simulation tools.

Gokhan Coskun is associate professor in the Department of Mechanical Engineering at Sakarya University. He received his BEng (2008), MSc (2010) and PhD (2014) from Sakarya University. He was a visitor researcher in the Internal Combustion Engine Division, Lund University, Sweden. He is working on combustion simulations, fuels and combustion studies in transport.

ORCID

Mehmet Salih Cellek http://orcid.org/0000-0001-5802-0715
Usame Demir http://orcid.org/0000-0001-7383-1428
Gokhan Coskun http://orcid.org/0000-0003-1485-4325

References

Alabaş, B., G. Tunç, M. Taştan, and İ. Yılmaz. 2021. Examination of combustion characteristics of oxygen enriched synthetic gases mixtures at various acoustic frequencies. *International Journal of Hydrogen Energy* 47 (24):12365–76. doi:10.1016/j.ijhydene.2021.07.035.

Alrbai, M., S. Al-Dahidi, and M. Abusorra. 2021. Investigation of the main exhaust emissions of HCCI engine using a newly proposed chemical reaction mechanism for biogas fuel. *Case Studies in Thermal Engineering* 26:100994. doi:10.1016/J.CSITE.2021.100994.

Alrbai, M., A. Darwish Ahmad, S. Al-Dahidi, A. M. Abubaker, L. Al-Ghussain, H. S. Hayajneh, and N. K. Akafuah. 2022. Effect of hydrogen sulfide content on the combustion characteristics of biogas fuel in homogenous charge compression ignition engines. *Case Studies in Thermal Engineering* 40:102509. doi:10.1016/j.csite.2022.102509.

Amar, H., M. Abdelbaki, T. Fouzi, and A. Zeroual. 2018. Effect of the addition of H2 and H2O on the polluting species in a counter-flow diffusion flame of biogas in flameless regime. *International Journal of Hydrogen Energy* 43 (6):3475–81. doi:10.1016/J.IJHYDENE.2017.11.159.

ANSYS FLUENT. 2018. V. 18.1. Canonsburg, PA: ANSYS Inc.

Bohlooli Arkhazloo, N., Y. Bouissa, F. Bazdidi-Tehrani, M. Jadidi, J. B. Morin, and M. Jahazi. 2019. Experimental and unsteady CFD analyses of the heating process of large size forgings in a gas-fired furnace. *Case Studies in Thermal Engineering* 14:14. doi:10.1016/J.CSITE.2019.100428.

Brookes, S. J., and J. B. Moss. 1999. Measurements of soot production and thermal radiation from confined turbulent jet diffusion flames of methane. *Combustion & Flame* 116 (1–2):49–61. doi:10.1016/S0010-2180(98)00027-3.

Cellek, M. S. 2020a. Turbulent flames investigation of methane and syngas fuels with the perspective of near-wall treatment models. *International Journal of Hydrogen Energy* 45 (60):35223–34. doi:10.1016/j.ijhydene.2020.05.039.

Cellek, M. S. 2020b. Flameless combustion modeling of CH4/H2 in the laboratory-scaled pilot furnace. *International Journal of Hydrogen Energy* 45 (60): 35208–35222.

Charest, M. R. J., Ö. L. Gülder, and C. P. T. Groth. 2014. Numerical and experimental study of soot formation in laminar diffusion flames burning simulated biogas fuels at elevated pressures. *Combustion & Flame* 161 (10):2678–91. doi:10.1016/J.COMBUSTFLAME.2014.04.012.

Colorado, A., and V. McDonell. 2018. Emissions and stability performance of a low-swirl burner operated on simulated biogas fuels in a boiler environment. *Applied Thermal Engineering* 130:1507–19. doi:10.1016/J.APPLTHERMALENG.2017.11.047.

Dai, W., C. Qin, Z. Chen, C. Tong, and P. Liu. 2012. Experimental studies of flame stability limits of biogas flame. *Energy Conversion and Management* 63:157–61. doi:10.1016/J.ENCONMAN.2012.03.021.

Deepanraj, B., N. Senthilkumar, and J. Ranjitha. 2019. Effect of solid concentration on biogas production through anaerobic digestion of rapeseed oil cake. *Energy Sources, Part A: Recovery, Utilization, and Environmental Effects* 43 (11):1329–36. doi:10.1080/15567036.2019.1636902.

Devi, S., N. Sahoo, and P. Muthukumar. 2023. Comparative performance evaluation of a porous radiant burner with a conventional burner: Biogas combustion. *Applied Thermal Engineering* 218:119338. doi:10.1016/J.APPLTHERMALENG.2022.119338.

Fischer, M., and X. Jiang. 2015. An investigation of the chemical kinetics of biogas combustion. *Fuel* 150:711–20. doi:10.1016/J.FUEL.2015.01.085.

Fuzesi, D., and V. Jozsa. 2019. Numerical analysis of biogas combustion in a lean premixed swirl burner. 7th International Youth Conference on Energy, IYCE 2019. doi:10.1109/IYCE45807.2019.8991563.

Habib, R., B. Yadollahi, A. Saeed, M. H. Doranehgard, L. Lkb, and N. Karimi. 2021. Unsteady ultra-lean combustion of methane and biogas in a porous burner – an experimental study. *Applied Thermal Engineering* 182:116099. doi:10.1016/J.APPLTHERMALENG.2020.116099.

Hoerlle, C. A., F. H. R. França, P. R. Pagot, and F. M. Pereira. 2020. Effects of radiation modeling on non-premixed sooting flames simulations under oxyfuel conditions. *Combustion & Flame* 217:294–305. doi:10.1016/J.COMBUSTFLAME.2020.04.012.

Hoerlle, C. A., and F. M. Pereira. 2019. Effects of CO2 addition on soot formation of ethylene non-premixed flames under oxygen enriched atmospheres. *Combustion & Flame* 203:407–23. doi:10.1016/J.COMBUSTFLAME.2019.02.016.

İlbaş, M., M. Şahin, and S. Karyeyen. 2018. 3D numerical modelling of turbulent biogas combustion in a newly generated 10 KW burner. *Journal of the Energy Institute* 91 (1):87–99. doi:10.1016/j.joei.2016.10.004.

Karataş, A. E., and Ö. L. Gülder. 2017. Effects of carbon dioxide and nitrogen addition on soot processes in laminar diffusion flames of ethylene-air at high pressures. *Fuel* 200:76–80. doi:10.1016/J.FUEL.2017.03.026.

Kekec, K. B., and S. Karyeyen. 2020. Combustion Characteristics on colorless distributed combustion (CDC) in a cyclonic burner. *International Journal of ENERGY STUDIES* 5:43–55.

Kekec, K. B., and S. Karyeyen. 2021. H2 – CH4 blending fuels combustion using a cyclonic burner on colorless distributed combustion. *International Journal of Hydrogen Energy* 47 (24):12393–409. doi:10.1016/j.ijhydene.2021.08.118.

Lehtomäki, A., S. Huttunen, and J. A. Rintala. 2007. Laboratory investigations on co-digestion of energy crops and crop residues with cow manure for methane production: Effect of crop to manure ratio. *Resources, Conservation & Recycling* 51:591–609. doi:10.1016/J.RESCONREC.2006.11.004.

Leung, T., and I. Wierzba. 2008. The effect of hydrogen addition on biogas non-premixed jet flame stability in a co-flowing air stream. *International Journal of Hydrogen Energy* 33 (14):3856–62. doi:10.1016/J.IJHYDENE.2008.04.030.

Liu, S., T. L. Chan, Z. He, Y. Lu, X. Jiang, and F. Wei. 2019. Soot formation and evolution characteristics in premixed methane/ethylene-oxygen-argon burner-stabilized stagnation flames. *Fuel* 242:871–82. doi:10.1016/J.FUEL.2018.12.051.

Liu, F., J. L. Consalvi, and F. Nmira. 2023. The importance of accurately modelling soot and radiation coupling in laminar and laboratory-scale turbulent diffusion flames. *Combustion & Flame* 258:112573. doi:10.1016/J.COMBUSTFLAME.2022.112573.

Liu, Z., and J. Lv. 2016. The effect of total solids concentration and temperature on biogas production by anaerobic digestion. *Energy Sources, Part A: Recovery, Utilization, and Environmental Effects* 38:3534–41. doi:10.1080/15567036.2016.1183064 .

Mameri, A., S. Boussetla, R. Belalmi, and Z. Aouachria. 2019. Combustion characterization of the mixtures biogas-syngas, strain rate and ambient pressure effects. *International Journal of Hydrogen Energy* 44 (39):22478–91. doi:10.1016/j.ijhydene.2019.05.142.

Mameri, A., and F. Tabet. 2016. Numerical investigation of counter-flow diffusion flame of biogas–hydrogen blends: Effects of biogas composition, hydrogen enrichment and scalar dissipation rate on flame structure and emissions. *International Journal of Hydrogen Energy* 41 (3):2011–22. doi:10.1016/j.ijhydene.2015.11.035.

Mong, G. R., M. C. Chiong, C. T. Chong, J. H. Ng, S. Mashruk, M. V. Tran, K. M. Lee, N. A. Samiran, K. Y. Wong, A. Valera-Medina, et al. 2023. Fuel-lean ammonia/biogas combustion characteristics under the reacting swirl flow conditions. *Fuel* 331:125983. doi:10.1016/J.FUEL.2022.125983.

Moussa, O., and Z. Driss. 2017. Numerical investigation of the turbulence models effect on the combustion characteristics in a non-premixed turbulent flame methane-air. *American Journal of Energy Research* 5:85–93. doi:10.12691/AJER-5-3-3.

Nourbakhsh, H., J. Rahbar Shahrouzi, A. Zamaniyan, H. Ebrahimi, and M. R. Jafari Nasr. 2018. A thermodynamic analysis of biogas partial oxidation to synthesis gas with emphasis on soot formation. *International Journal of Hydrogen Energy* 43 (33):15703–19. doi:10.1016/J.IJHYDENE.2018.06.134.

Özdemir, M. R., M. U. Yangaz, and I. T. Yilmaz. 2021. Energy, exergy and exergo-economic characteristics of hydrogen enriched hydrocarbon-based fuels in a premixed burner. *Energy Sources, Part A: Recovery, Utilization, and Environmental Effects* 43 (23):3119–36. doi:10.1080/15567036.2021.1895371.

Rocha, N., F. M. Quintino, and E. C. Fernandes. 2020. H2 enrichment impact on the chemiluminescence of biogas/air premixed flames. *International Journal of Hydrogen Energy* 45 (4):3233–50. doi:10.1016/J.IJHYDENE.2019.11.115.

Sabnis, P., and S. K. Aggarwal. 2018. A numerical study of NOx and soot emissions in methane/n-heptane triple flames. *Renew Energy* 126:844–54. doi:10.1016/J.RENENE.2018.04.007.

Şanlı, A., İ. T. Yılmaz, and M. Gümüş. 2021. Investigation of combustion and emission characteristics in a TBC diesel engine fuelled with CH4–CO2–H2 mixtures. *International Journal of Hydrogen Energy* 46 (47):24395–409. doi:10.1016/j.ijhydene.2021.05.014.

Sarvestani, N. S., M. H. Abbaspour-Fard, M. Tabasizadeh, H. Nayebzadeh, T. C. Van, M. Jafari, Z. Ristovski, and R.J. Brown. 2020. Synthesize of magnetite Mg-Fe mixed metal oxide nanocatalyst by urea-nitrate combustion method with optimal fuel ratio for reduction of emissions in diesel engines. *Journal of Alloys and Compounds* 838:155627. doi:10.1016/J.JALLCOM.2020.155627.

Smith, G. P., D. M. Golden, M. Frenklach, N. W. Moriarty, B. Eiteneer, M. Goldenberg, C. T. Bowman, R. K. Hanson, S. Song, W. C. Gardiner Jr, et al. n.d. Gri-mech 3.0.

Tang, B., M. He, Y. Dong, J. Liu, X. Zhao, C. Wang, K. Wu, F. Yin, and W. Zhang. 2020. Effects of different forms of vegetable waste on biogas and methane production performances in a batch anaerobic digestion reactor. *Energy Sources, Part A: Recovery, Utilization, and Environmental Effects* 1–11. doi:10.1080/15567036.2020.1818003.

Unitrove. 2021. https://www.unitrove.com/engineering/tools/gas/natural-gas-calorific-value.

Wei, Z., H. Zhen, C. Leung, C. Cheung, and Z. Huang. 2020. Effects of H2 addition on the formation and emissions of CO/NO2/NOx in the laminar premixed biogas-hydrogen flame undergoing the flame-wall interaction. *Fuel* 259:116257. doi:10.1016/J.FUEL.2019.116257.

Yang, X., Z. He, S. Dong, and H. Tan. 2018. Prediction of turbulence radiation interactions of CH4–H2/air turbulent flames at atmospheric and elevated pressures. *International Journal of Hydrogen Energy* 43 (32):15537–50. doi:10.1016/j.ijhydene.2018.06.060.

Yilmaz, İ., B. Alabaş, M. Taştan, and G. Tunç. 2020. Effect of oxygen enrichment on the flame stability and emissions during biogas combustion: An experimental study. *Fuel* 280:280. doi:10.1016/j.fuel.2020.118703.

Yilmaz, H., O. Cam, S. Tangoz, and I. Yilmaz. 2017. Effect of different turbulence models on combustion and emission characteristics of hydrogen/air flames. *International Journal of Hydrogen Energy* 42 (40):25744–55. doi:10.1016/j.ijhydene.2017.04.080.

Yilmaz, I., and M. Ilbas. 2008. An experimental study on hydrogen–methane mixtured fuels. *International Communications in Heat and Mass Transfer* 35 (2):178–87. doi:10.1016/j.icheatmasstransfer.2007.06.004.

Zhen, H. S., C. W. Leung, and C. S. Cheung. 2013. Effects of hydrogen addition on the characteristics of a biogas diffusion flame. *International Journal of Hydrogen Energy* 38 (16):6874–81. doi:10.1016/J.IJHYDENE.2013.02.046.

Zhen, H. S., C. W. Leung, C. S. Cheung, and Z. H. Huang. 2016. Combustion characteristic and heating performance of stoichiometric biogas–hydrogen–air flame. *International Journal of Heat and Mass Stansfer* 92:807–14. doi:10.1016/J.IJHEATMASSTRANSFER.2015.09.040.

Zouagri, R., A. Mameri, F. Tabet, and A. Hadef. 2020. Characterization of the combustion of the mixtures biogas-syngas at high strain rates. *Fuel* 271:117580. doi:10.1016/j.fuel.2020.117580.